

# Investigation of microstructure and mechanical properties of titanium alloy sheet using low power Nd-YAG laser welding process

U. Kumar<sup>1</sup>, D. K. Gope<sup>1</sup>, R. Kumar<sup>2\*</sup>, S. Chattopadhyaya<sup>1</sup>, A. K. Das<sup>1</sup>, A. Pramanik<sup>3</sup>, G. Krolczyk<sup>4</sup>

<sup>1</sup>*Indian Institute of Technology (ISM) Dhanbad, India*

<sup>2</sup>*Department of Mechanical Engineering, Birla Institute of Technology, Mesra, Ranchi, India*

<sup>3</sup>*Department of Mechanical Engineering, Curtin University, Bentley, WA 6102, Australia*

<sup>4</sup>*Department of Manufacturing Engineering and Automation, Opole University of Technology, Opole, Poland*

Received 6 February 2017, received in revised form 30 October 2017, accepted 20 March 2018

## Abstract

In the present investigation, welding of 1 mm thick Ti-6Al-4V sheet has been done by Pulsed Wave (PW) Nd-YAG laser with a variation of laser power from 100 to 400 W and welding speed from 4 to 6 mm s<sup>-1</sup>. The microstructure and microhardness of the fusion zone indicate that the finely serrated and regular plate-shaped microstructures and the resultant hardness in the welds are the key factors behind the enhanced tensile strength of all joints. The weld bead size increases with decreasing welding speed and vice versa. The hardness increases around the heat affected zone as compared to that of the parent metal, and it is the maximum at the centre of the welded region. In the investigation, the tensile strength of specimen with different process parameters has been found to be approximately equal to the tensile strength of the parent metal. In XRD analysis, the weld zone has been found to consist of 78 %  $\alpha$  and 22 %  $\beta$  peaks where two  $\beta$ -titanium peaks (bcc) 100 occur at 39.5110° and 56.9120°.

**Key words:** microstructure, microhardness, pulsed wave laser, tensile strength

## 1. Introduction

In recent years, titanium alloys have become one of the most widely used materials in the field of metallurgical research. Among all the titanium alloys, the Ti-6Al-4V alloy has emerged to be the most popular material [1, 2]. Thin sheets of Ti6Al4V are widely used in turbine disks, compressor blades, airframes, rings for jet engines, pressure vessels, rocket engine cases, helicopter rotor hubs, medical and surgical devices, air inlets, fuel tanks, etc. Again, titanium capsules that contain Iodine-125 radioisotope are widely used for cancer radiotherapy [3, 4]. Ti-6Al-4V is a two-phase  $\alpha + \beta$  alloy with aluminium as the alpha stabilizer and vanadium as the beta stabilizer. Due to its high strength and low density along with good mechanical properties, it can withstand temperature even up to 450 °C. This alloy can be strengthened by heat treatment or by thermo-mechanical processing.

It is also possible to instil the best suitable properties in Ti-6Al-4V by solution heat treatment [5]. The work of Ruggiero et al. investigated the friction and wear behaviour of ultra-high molecular weight polyethylene sliding against TiAl6V4 alloy, against AISI316L austenitic stainless steel and against Al<sub>2</sub>O<sub>3</sub> ceramic under dry and lubricated conditions. The results show that the AISI316L austenitic stainless steel and TiAl6V4 alloy have marked in dry conditions better values in the friction coefficient and the friction force [6].

Nd-YAG pulsed wave laser welding is considered to be the most suitable method for welding because of its ability to control heat input with greater precision and to reduce the heat-affected zone (HAZ), thereby enhancing mechanical properties of the welded joint [7–9]. Earlier, for thin sheets of titanium alloys, TIG welding was the most widely used method. However, its main disadvantage is the very high amount of heat

\*Corresponding author: tel.: 917545095465; e-mail address: [ratana\\_876@yahoo.co.in](mailto:ratana_876@yahoo.co.in)

input resulting in distortions [10, 11]. Gursel et al. studied about the crack risk of Ti-6Al-4V using Nd-YAG pulsed laser. The result shows that by controlling the process parameter and heat input, the destruction of titanium alloys can be prevented [12]. Kumar et al. [13] investigated the influence of process parameter on melt profile and characteristics of pulsed laser treated Ti-6Al-4V. The results show that by controlling the peak power, average power and welding speed, significant reduction in hardness could be achieved. Kabir et al. worked on the defocusing distance and welding speed influence on transverse weld bead geometry, and his result shows that to get quality weld joint with low welding defects both parameters could be optimized [14]. Another important aspect of this process is shielding gas protection to improve the mechanical properties by preventing oxide formation and other impurities in the welded piece during the laser welding process [15–17].

X. Cao et al. [18] used annealed Ti-6Al-4V alloy sheets of 1 and 2 mm thickness with 4 kW laser power during the welding process. The results show that loss of ductility depends on the presence of micropores and aluminium oxide inclusions. Torkamany et al. studied the effect of process parameters on keyhole behaviour of welding using a 400W Nd-YAG pulsed laser setup. It was found that the formation of the keyhole is highly dependent on laser pulse parameters [19]. Gao et al. examined the effect of overlapping factor on the microstructures and mechanical properties using pulsed Nd-YAG laser welded Ti6Al4V alloy sheets. The result indicates that by increasing the overlapping factor, the grains in the fusion zone become coarser, and the width of the weld bead increases [20]. During the welding process, various parameters, such as laser power, welding speed, power density, beam diameter, pulse width, pulse repetition rate, pulse energy, gas flow rate, defocusing distance, beam angle, etc., can be varied to get the best quality of the laser welding [21]. High power continuous wave mode solid-state Nd-YAG lasers are widely used in aerospace industry. The observations made so far indicate that there has not been much study on the low power pulsed Nd-YAG laser welding of Ti-6Al-4V alloys though this method has clear advantages over other methods. In the present work, the focus is largely on the effect of combining laser power and welding speed of low power pulsed Nd-YAG laser on the quality of welded joints of the Ti-6Al-4V alloy.

## 2. Experimental procedures and material

### 2.1. Experimental material and its mechanical properties

In the present work, a Ti-6Al-4V sheet with a

Table 1. Mechanical properties of titanium alloy (Ti-6Al-4V)

Tensile strength (MPa)	Yield strength (MPa)	Elongation (%)	Hardness, HV
964 ± 42	891 ± 39	14	356

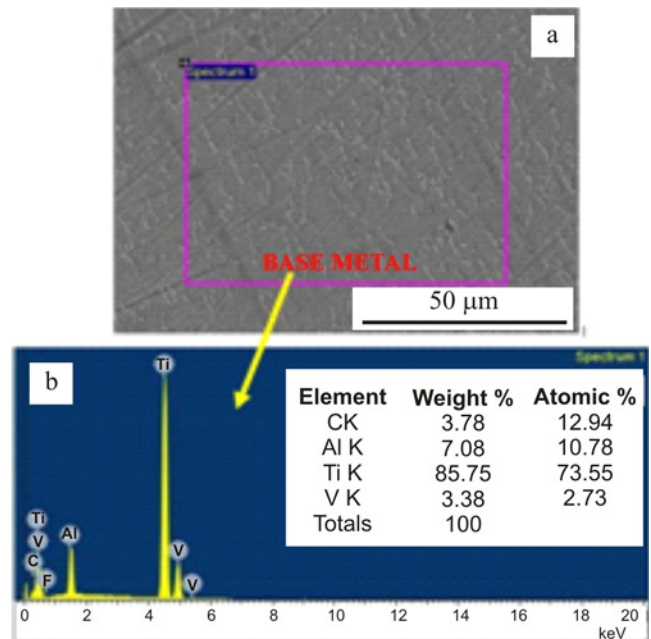


Fig. 1. EDX analysis of the titanium alloys (Ti-6Al-4V).

thickness of 1 mm was used for welding. The chemical composition (wt.%), learnt from the EDX analysis, and the mechanical properties of the Ti-6Al-4V material are mentioned in Fig. 1 and Table 1 consecutively.

### 2.2. Experimental setup for laser welding

A 400 W Nd-YAG laser was used to weld the thin Ti-6Al-4V sheet. The laser welding head was mounted on a robotic arm. The spot diameter of the laser beam was 0.45 mm with a focal length of 190 mm. Argon was used as the shielding gas. As argon has a higher density than helium, nitrogen and atmospheric air, it is more convenient to use argon as a shielding gas. The complete experimental setup with a sample dimension of 165 mm × 100 mm × 1 mm is shown in Fig. 2.

To ensure superior laser welding quality, direct parameters, such as laser power ( $P$ ) and welding speed ( $v$ ), were altered. The shielding gas had a flow rate of 8 l min<sup>-1</sup>, a standoff distance of 3 mm and a welding speed of 4 to 6 mm s<sup>-1</sup>. In the present work, 1 mm thick titanium alloy sheet was used in butt-welded configuration with power ranging from 40 to

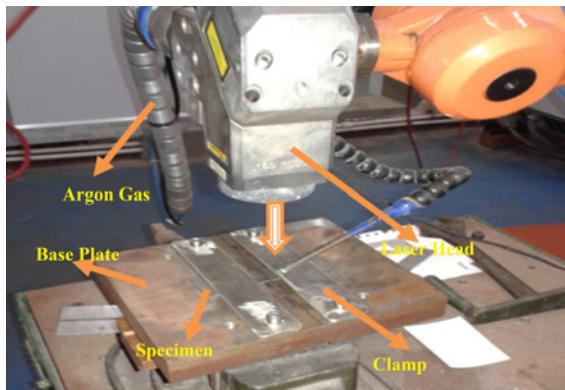


Fig. 2. Photographic view of Nd: YAG laser welding experimental setup.

Table 2. Constant weld parameters used in the present study

Wavelength	1.06 $\mu\text{m}$
Pulse energy	20 J
Peak pulse power	1000 W
Pulse duration	20 ms
Pulse frequency	20 Hz
Spot diameter	0.45 mm

Table 3. Welding parameters used in the present study

Sample	Average power (W)	Welding speed ( $\text{mm s}^{-1}$ )
a	160	4
b	160	6
c	192	4
d	192	6
e	202	4
f	202	6

400 W. The Ti-6Al-4V material is annealed, where two phases ( $\alpha$  &  $\beta$ ) are present simultaneously. The constant welding parameters, used in the present study, are given in Table 2. The thin Ti-6Al-4V sheets were brushed and cleaned with acetone just before the welding process. A focusing lens (focal length 190 mm) was used to deliver the beam to the samples. Table 3 presents the weld parameters used in the present study.

Two sheets of the same material and size were fixed on the table of the welding machine just below the laser head as shown in Fig. 2. For proper alignment, all the four corners of both the thin sheets were kept at a right angle. The edges were aligned properly and kept below the head of the laser beam. Next, whether

the sheets were perfectly aligned or not, was checked by viewing the alignment through the lens. Then the laser spot was manually run on the line of contact of the two sheets to check whether the laser beam would incident on the line of contact or not. In case of any mismatch, the alignments of the sheets with the laser beam trajectory were adjusted. After proper alignment and clamping, the two sheets were welded.

The plates were mechanically brushed and cleaned with acetone before welding. Initially, a few welding tests were conducted to attain suitable values of process parameters regarding full penetration and high-quality fusion zones. For certain time, power was kept constant and welding speed varying, while for certain another period, the welding speed was kept constant and power varying. From the results of several welding tests, seven combinations of laser power and welding speed were selected by their full penetration capability and fusion zones as shown in Table 3. A large number of welding samples were needed for satisfactory evaluation of weld properties. For assessment, these samples were polished by standard grinding machine and chemically etched by reagents.

### 2.3. Surface morphology observation

The sections perpendicular to the welding direction were cut for morphologic observation and then subjected to several steps of machine polishing. The cross-sections of the laser welds were then etched using a Kroll's reagents solution (2 ml HF, 1.5 ml HCl, 6 ml  $\text{HNO}_3$  and 90 ml  $\text{H}_2\text{O}$ ) for 20 s. Microstructure analysis was done by an optical microscope (OM) and field emission scanning electron microscopy (FESEM).

### 2.4. Microhardness measurement process

The Vickers hardness machine (Economet VH-1 MD) was used for microhardness measurement of the Nd-YAG laser-welded samples, using an indentation load of 100 gf and in a dwell time of 10 seconds at room temperature. Before taking the microhardness measurement, the samples were polished properly. The measurements were taken along the length of the specimen, keeping the weld zone as the centre. Multiple measurements were taken to make allowance for the variation of hardness values in the test samples.

### 2.5. Tensile test measurement process

In the present work, the tensile test specimens were prepared as per the prescribed standard in ASTM E-8. The weld samples contained part of the HAZ with fusion zone at the centre of the Nd-YAG laser weld, as shown in Fig. 3. A fully automated closed loop servo mechanical tensile testing machine [BISS], having a load capacity of 25 kN, was used. The ten-

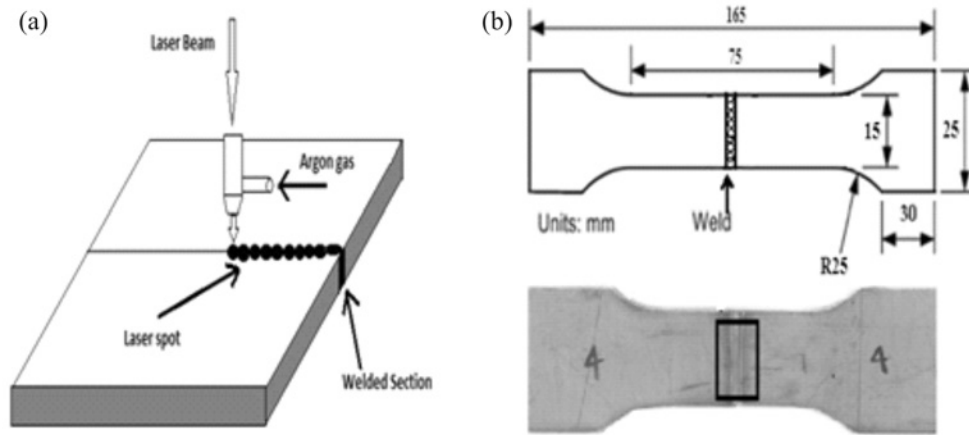


Fig. 3. (a) Representation of the pulsed spot laser welding; (b) tensile specimen (thickness: 1 mm).

side tests were conducted at room temperature. The test samples were deformed at a constant strain rate of  $0.0001\text{ s}^{-1}$ . At the gauge section of the specimen, an axial extensometer (12.5 mm gauge length) was attached using rubber bands. All the data were provided as computer output by the control unit of the tensile test machine. The average value of all the data was taken for calculating the result. Tensile data of the Nd-YAG laser-welded samples at different combinations of welding speed and laser power were measured and recorded.

### 3. Results and discussion

#### 3.1. Effect of Nd-YAG laser welding parameters on the laser weld bead quality

During the last few years, many important parameters have been tried and tested to obtain a good Nd-YAG laser welding quality. It has been found to strictly depend upon external parameters, such as good penetration, smoothness of the weld bead and width of the welded zone. A cross-sectional view of the Nd-YAG laser weld beads at different combinations of laser power and welding speed are shown in Fig. 4. Figures 4a–f show the front side view and Figs. 4a1–f1 show the root side view of the laser weld beads with different combinations of laser power and welding speed, i.e., (a) with power 160 W and welding speed  $4\text{ mm s}^{-1}$ , (b) with power 160 W and welding speed  $6\text{ mm s}^{-1}$ , (c) with power 192 W and welding speed  $4\text{ mm s}^{-1}$ , (d) with power 192 W and welding speed  $6\text{ mm s}^{-1}$ , (e) with power 202 W and welding speed  $4\text{ mm s}^{-1}$ , (f) with power 202 W and welding speed  $6\text{ mm s}^{-1}$ . It is clear from Fig. 4 that widths of the weld bead vary with variation of parameters. At the root of the Nd-YAG laser welds, the penetration depth also varies with variation in the welding parameters.

In Fig. 4c, there is a certain amount of spatter in

the welded zone as well as near the base of the material surface. The widths of the Nd-YAG laser welded joints in Figs. 4a–f are 1.83, 1.56, 1.45, 1.97, 1.83, and 1.62 mm, respectively. It indicates that the width of the weld zone is minimum in case of sample (c), i.e., with power 192 W and welding speed  $4\text{ mm s}^{-1}$ . In the present study, the laser spot diameter was 0.45 mm, which not only had a major influence on the width of the laser weld surface but also on the incident angle of the laser beam. During the investigation, the laser incident direction was vertical.

Figures 4c1,d1 show the black surface with a high amount of spatter in the weld bead zone. At the root side, the surface finish is not as good as that of the front side. Out of these figures, the surface finish in Fig. 4e1, with power 202 W and welding speed  $4\text{ mm s}^{-1}$ , is smooth and plain. The widths of the welded joints at the root side in Figs. 4a1–f1 are 1.70, 1.46, 1.41, 1.83, 1.66, and 1.69 mm, respectively. It also indicates that the width of the back side of the welded joint is the minimum in case of the sample (c) with power 192 W and welding speed  $4\text{ mm s}^{-1}$ . From these experiments, the appropriate Nd-YAG laser welding parameter combination that one gets is laser power 192 W and welding speed  $4\text{ mm s}^{-1}$ .

#### 3.2. Morphology of the joint

Figure 5a shows the optical microscopic image while Figs. 5b–d show the FESEM image of the top surface of the welded zone in the sample. Figure 5a indicates three zones of the weld region, i.e., FZ (fusion zone), HAZ and BM (base metal), in which the HAZ is very narrow in comparison to the FZ. From the figure, it is also clear that the crystal microstructure of the BM is entirely different from the microstructure of the weld zone. During cooling, acicular or needle alpha is the most common transformation phase, formed from beta. Moreover, if the cooling rate is very high, an acicular  $\alpha'$  martensite formation takes place. Due to the

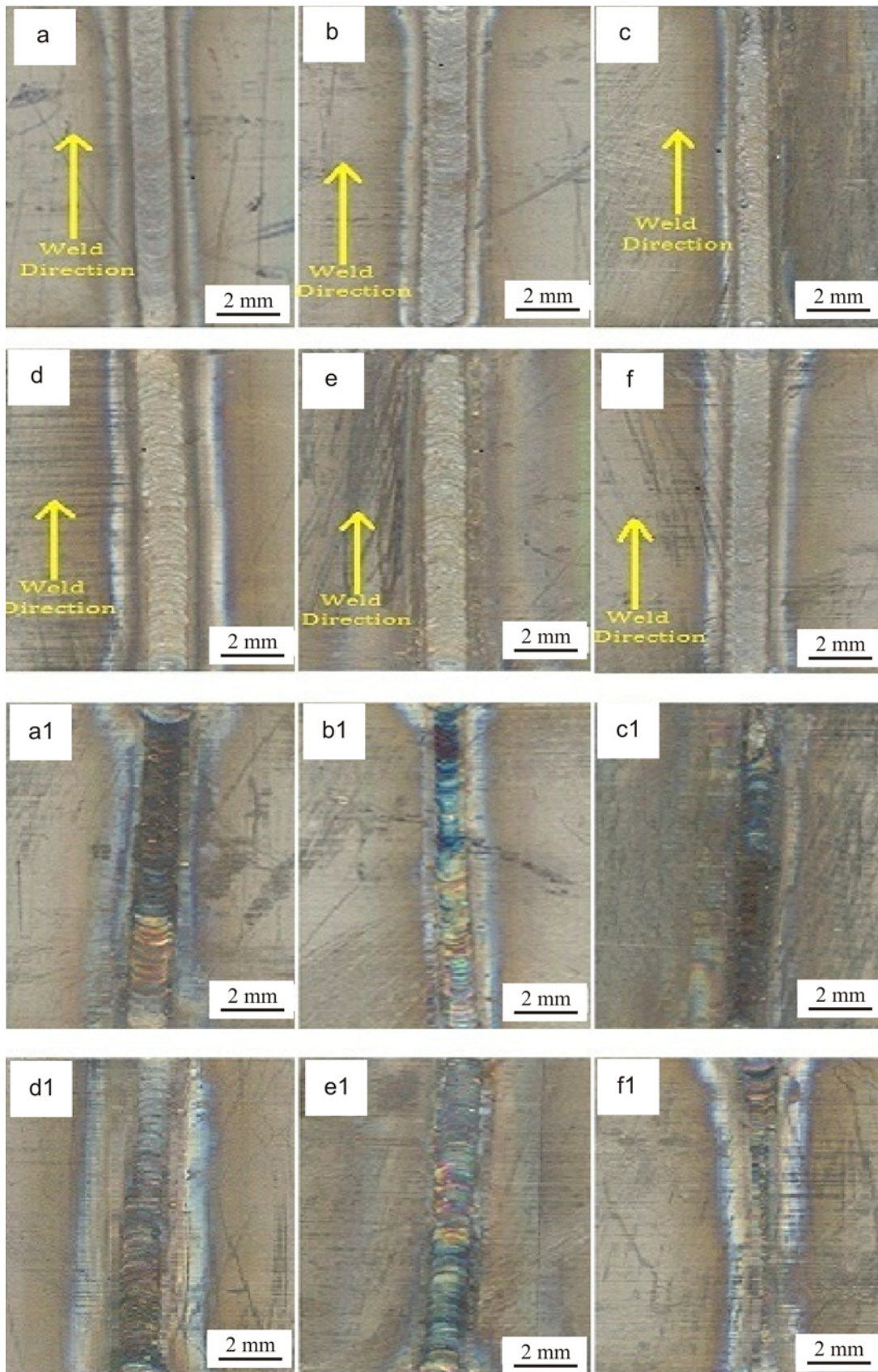


Fig. 4. Typical front side view of the Nd:YAG laser welds with different parameters: (a)  $P = 160 \text{ W}$ ,  $v = 4 \text{ mm s}^{-1}$ ; (b)  $P = 160 \text{ W}$ ,  $v = 6 \text{ mm s}^{-1}$ ; (c)  $P = 192 \text{ W}$ ,  $v = 4 \text{ mm s}^{-1}$ ; (d)  $P = 192 \text{ W}$ ,  $v = 6 \text{ mm s}^{-1}$ ; (e)  $P = 202 \text{ W}$ ,  $v = 4 \text{ mm s}^{-1}$ ; and (f)  $P = 202 \text{ W}$ ,  $v = 6 \text{ mm s}^{-1}$ . Figures a1–f1 are the root side view of samples a–f, respectively.

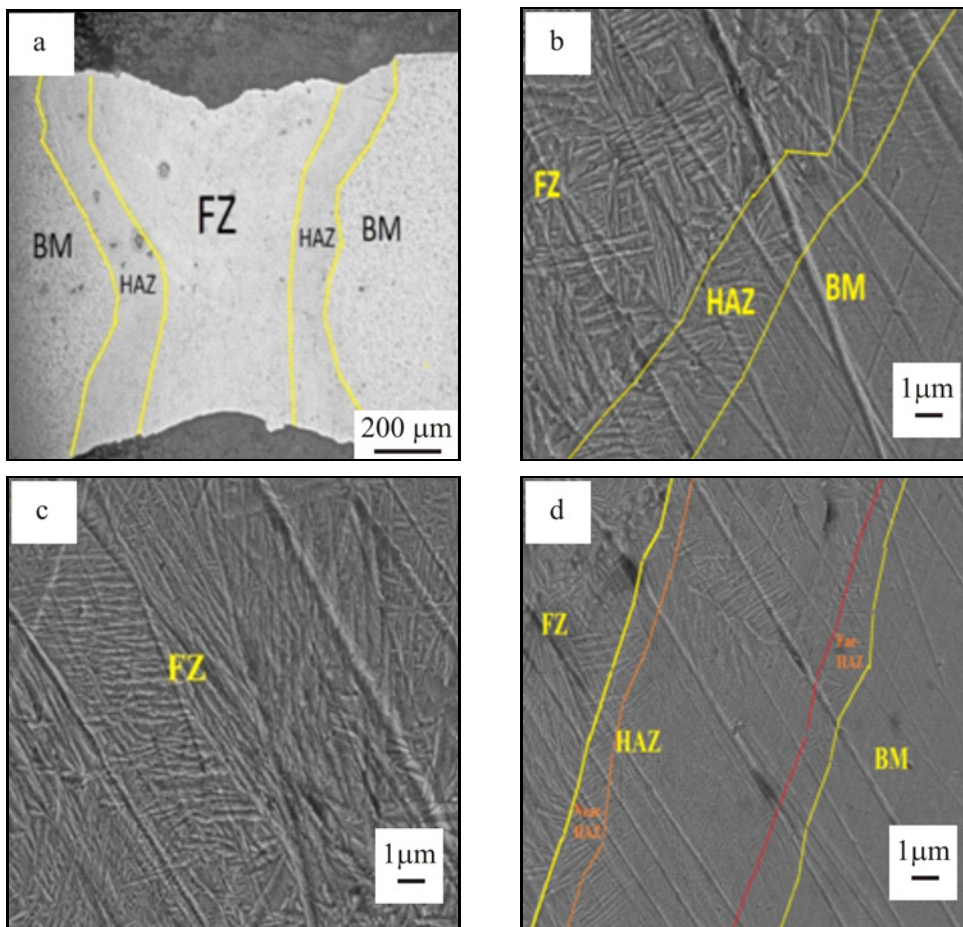


Fig. 5. Joint morphology of titanium alloys sample in (a), (b), (c), and (d).

formation of fine acicular martensite, the weld bead possesses a high value of hardness but the relatively low value of ductility. The boundary layer between the BM and HAZ shows how the temperature distribution and complex thermal cycle operates to change the microstructure during laser welding. The crystal microstructure of the HAZ is acicular or lamellar alpha in Fig. 5b. In the granular region, the microstructure also consists of elongated  $\alpha$  and  $\beta$  lamellae.

Compared to the grains of the HAZ there is an occasional change in the grains of the FZ. Figure 5c shows microstructure of the FZ, detected through the FESEM at a magnification of 4KX. Acicular grains appear in the FZ with high-temperature phase grain boundaries. Moreover, a retained  $\beta$ -phase can be observed, becoming the only dominant phase with a significant amount of equiaxed morphology. The FZ of the melt pool, developed by Nd-YAG laser welding, contains a high degree of needle-shaped phases in the martensitic  $\alpha$  matrix. These needle-shaped phases are in the martensitic  $\alpha$  matrix of the localized region in the FZ where beta stabilizers lower the beta transus, thereby changing the mechanical properties.

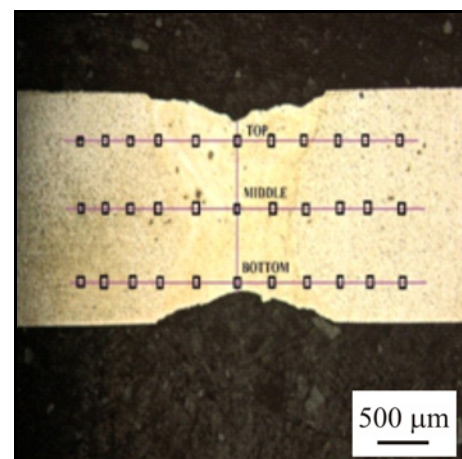


Fig. 6. Transverse sections of 1-mm welded joint.

### 3.3. Microhardness analysis

Figure 6 shows the distribution of microhardness measurement on the cross-section of the laser welding sample at the top section, middle section, and bottom

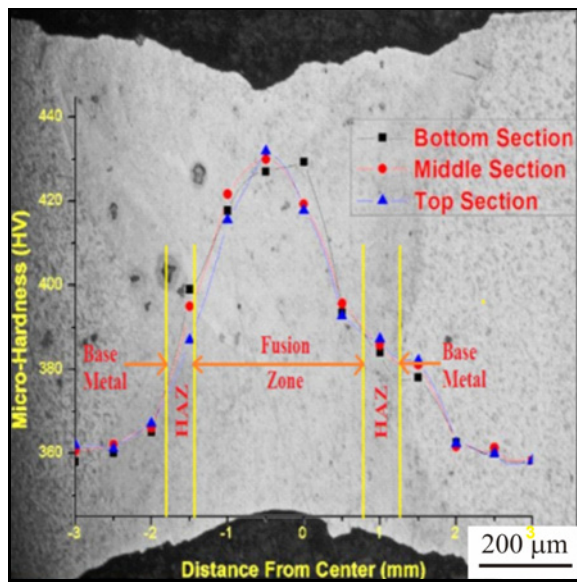


Fig. 7. Microhardness profiles across weld centre line.

section. Figure 7 shows the typical microhardness distribution profile at the transverse sections of the welds. The profile in Fig. 7 indicates the microhardness variations in all the three sections. The value of microhardness is the lowest at the BM, which is around  $350 \pm 5$  HV while it is the highest at the FZ. In general, the FZ shows 15 to 18% higher microhardness value as compared to the BM value in every combination of welding speed and laser power. The variation of microhardness highly depends upon high cooling rate. The high cooling rate promotes the uneven growth of the grains. Due to this inhomogeneous grain growth, the complete transformation into the martensite structure does not take place. The higher value of microhardness in the FZ also depends upon the martensitic  $\alpha$  structure which ensures high strength and hardness. Acicular martensite phase  $\alpha$  structure is found maximum near the fusion layer, and the percentage of the acicular martensite  $\alpha$  grain decreases gradually from the fusion layer. Finally, it is almost absent at the BM and the HAZ interface.

In comparison, the average value of microhardness at the top section of the weld is higher than that of the middle and the bottom sections. However, there is no clear trend in these sections as regards the relation between microhardness and the welding speed. In all the three sections, the microhardness is almost uniform in the BM region.

### 3.4. Tensile strength analysis

Many welded samples, including the BM, were tested according to the exact conditions of the ISO Standard. Among all the tensile strength data, the

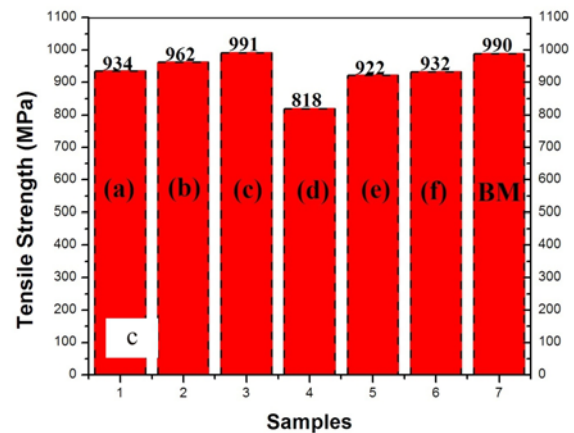
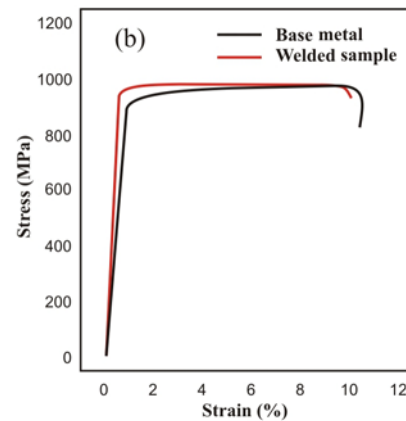
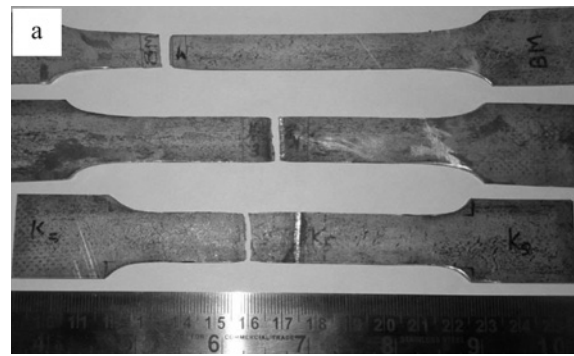


Fig. 8. (a) Tensile samples of the titanium alloy after the tensile test; (b) stress-strain curve of the (Ti-6Al-4V); and (c) represents the ultimate tensile strength of the samples.

most credible ones were taken and compared with the BM tensile strength data. Figure 8a shows the pictorial view of the samples after the tensile test. Figure 8b shows the stress-strain curves of the Nd-YAG laser weld sample and the BM. Figure 8c indicates the comparison of the welded samples and the BM of ultimate tensile strength. From the bar chart, it is clear that the tensile strength values of the Nd-YAG laser welds are equal to that of the BM values. In this study, the obtained values of the tensile strength of the Nd-YAG laser welded samples were found to range from 954 to 989 MPa.

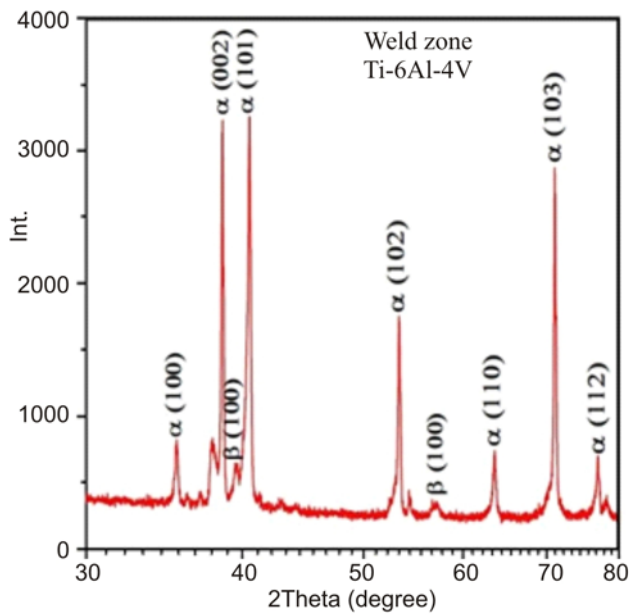


Fig. 9. XRD pattern for the welded zone.

The area under the stress-strain curve in the Nd-YAG laser weld is slightly larger than that of the BM. High heat input in the fusion zone results in the formation of finer grains. Finer grains are responsible for the enhancement of the tensile strength. In general, it can be concluded that the tensile properties of the welded joints primarily depend on the microstructure. It is very clear that the microstructure grains of the Nd-YAG laser welding zone are entirely different from the grains of the BM. The enhancement in the tensile strength of the welding zone is mainly due to the equiaxed finer grains of the  $\beta$ -phase. The coarse grains in the BM manifest the low tensile strength as compared with the weld metal.

### 3.5. XRD pattern analysis

Figure 10 shows the XRD pattern in the as-received material. The diffraction patterns were recorded using a high-resolution XRD between angles  $30^\circ$  and  $80^\circ$ . As there are few references and less information in the JCPDS (Joint Committee on Powder Diffraction Standards) data, a detailed comparison could not be attempted here. Figure 9 shows the XRD pattern of the Nd-YAG laser welded zone. From Fig. 10, by the qualitative fitting of the as-received material, the  $\alpha$ -phase is characterized by (100), (002), (101), (102), (110), (103), (112), and (201) reflections.

The detector was placed 100 mm behind the weld. At 12.0 keV, this  $2\theta$  range covers two possible  $\beta$ -titanium peaks (bcc), i.e., 100 at an angle of  $39.511^\circ$ , (bcc) 100 at an angle of  $56.912^\circ$  and seven possible  $\alpha$ -titanium (hcp) peaks. The seven  $\alpha$  peaks were at an

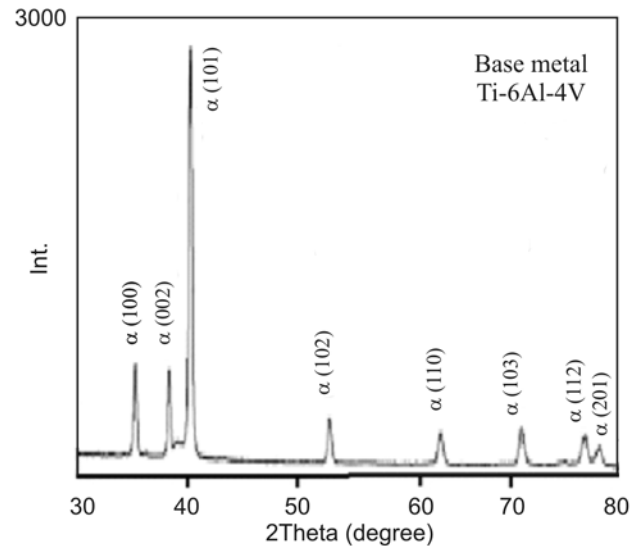


Fig. 10. XRD pattern for the as-received (Ti-6Al-4V).

angle of (100)  $35.375^\circ$ , (002)  $38.558^\circ$ , (101)  $40.488^\circ$ , (102)  $53.324^\circ$ , (110)  $63.566^\circ$ , (103)  $71.045^\circ$ , and (112)  $77.018^\circ$ . In Fig. 9, two  $\beta$ -titanium peaks (bcc) and seven  $\alpha$ -titanium (hcp) peaks can be found. It is clear from the above data that the alloy contains approximately 78% of  $\alpha$  peaks and 22% of  $\beta$  peaks at room temperature. The diffraction pattern of Nd-YAG laser welding zone is dominated by the hcp diffraction peaks. It is clear that the extent of  $\beta$ -phase increases during heating, leading to complete transformation of alloys to the  $\beta$ -phase at a temperature of  $958^\circ\text{C}$ .

## 4. Conclusions

Thin Ti-6Al-4V sheets, having 1 mm thickness, were welded by using a 400 W Nd:YAG laser machine. In the present study, the effects of welding on the surface morphology, microstructures, hardness and tensile properties were investigated at different combinations of welding power and welding speed. Following are the basic observations, derived from the investigation:

- No solidification of cracks can be found in the FZ although certain overheated points can be found in the HAZ.

- The presence of finely serrated and regular plate-shaped grains along with the resultant hardness in the Nd:YAG joints are the main factors for improving the tensile strength of this joint.

- The XRD pattern shows the Nd-YAG laser welding zone containing 78% of  $\alpha$  peaks and 22% of  $\beta$  peaks. Two  $\beta$ -titanium peaks (bcc) 100 at an angle of  $39.511^\circ$  and (bcc) 100 at an angle of  $56.912^\circ$  are formed in the weld zone during solidification.

- The microhardness is higher in the FZ than in

the HAZ and the BM region. It is in the BM region where one gets the lowest microhardness.

– The welded sample prepared at the 192 W power and welding speed  $4 \text{ mm s}^{-1}$  has the minimum weld bead on the front side as well as at the root side as compared to the other samples. Moreover, it has the almost equal ultimate tensile strength than that of BM.

## References

- [1] Caiazzo, F., Curcio, F., Daurelio, G., Minutolo, F. M. C.: *Journal of Materials Processing Technology*, 149, 2004, p. 546. [doi:10.1016/j.jimatprotec.2003.12.026](https://doi.org/10.1016/j.jimatprotec.2003.12.026)
- [2] Casalino, G., Curcio, F., Minutolo, F. M. C.: *Journal of Materials Processing Technology*, 167, 2005, p. 422. [doi:10.1016/j.jimatprotec.2005.05.031](https://doi.org/10.1016/j.jimatprotec.2005.05.031)
- [3] Li, Z., Gobbi, S. L., Norris, I., Zolotovskiy, S., Richter, K. H.: *J. Mater Process Technology*, 65, 1997, p. 203. [doi:10.1016/S0924-0136\(96\)02263-7](https://doi.org/10.1016/S0924-0136(96)02263-7)
- [4] Lee, H. K., Han, H. S., Son, K. J., Hong, S. B.: *Mater Sci Eng A*, 415, 2006, p. 149. [doi:10.1016/j.msea.2005.09.059](https://doi.org/10.1016/j.msea.2005.09.059)
- [5] Maruda, R. W., Krolczyk, G. M., Michalski, M., Nieslony, P., Wojciechowski, S.: *Journal of Materials Engineering and Performance*, 26, 2017, p. 431. [doi:10.1007/s11665-016-2450-4](https://doi.org/10.1007/s11665-016-2450-4)
- [6] Wang, S. H., Wei, M. D., Tsay, L. W.: *Materials Letters*, 57, 2003, p. 1815. [doi:10.1016/S0167-577X\(02\)01074-1](https://doi.org/10.1016/S0167-577X(02)01074-1)
- [7] Ruggiero, A., D'Amato, R., Gómez, E., Merola, M.: *Tribology International*, 96, 2016, p. 349. [doi:10.1016/j.triboint.2015.12.041](https://doi.org/10.1016/j.triboint.2015.12.041)
- [8] Baghjari, S. H., Mousavi, S. A. A. A.: *Mater Des*, 43, 2013, p. 1. [doi:10.1016/j.matdes.2012.06.027](https://doi.org/10.1016/j.matdes.2012.06.027)
- [9] Mousavi, S. A. A. A., Sufizadeh, A. R.: *Mater Des*, 30, 2009, p. 3150. [doi:10.1016/j.matdes.2008.11.026](https://doi.org/10.1016/j.matdes.2008.11.026)
- [10] Zhang, J. X., Xue, Y., Gong, S. L.: *SciTechnol Weld Join*, 10, 2005, p. 643. [doi:10.1179/174329305X48374](https://doi.org/10.1179/174329305X48374)
- [11] Baeslack, W. A., Gerken, J. M., Cross, C., Hanson, J., Liu, P. S., Monses, J. C., Schley, J., Showalter, L.: *Welding Handbook*. 8th Edition. Miami, American Welding Society 1998.
- [12] Lathabai, S., Jarvis, B. L., Barton, K. J.: *Mater. Sci. Eng. A*, 299, 2001, p. 81. [doi:10.1016/S0921-5093\(00\)01408-8](https://doi.org/10.1016/S0921-5093(00)01408-8)
- [13] Gursel, A.: *Materials Letters*, 197, 2017, p. 233. [doi:10.1016/j.matlet.2016.12.112](https://doi.org/10.1016/j.matlet.2016.12.112)
- [14] Kumar, V. C.: *Journal of Surface & Coatings Technology*, 201, 2006, p. 3174. [doi:10.1016/j.surfcoat.2006.06.035](https://doi.org/10.1016/j.surfcoat.2006.06.035)
- [15] Kabir, A. S. H., Cao, X., Medraj, M., Wanjara, P., Cuddy, J., Birur, A.: In: *Proceedings of Conference of the Materials Science and Technology (MS&T)*. Houston, ASM International 2010, p. 2787.
- [16] Wang, H., Shi, Y., Gong, S., Duan, A.: *J. Mater. Process. Technology*, 184, 2007, p. 379. [doi:10.1016/j.jimatprotec.2006.12.014](https://doi.org/10.1016/j.jimatprotec.2006.12.014)
- [17] Gerevey, D., Sallamand, P., Cicala, E., Ignat, S.: *Opt. Laser Technol*, 37, 2005, p. 647. [doi:10.1016/j.optlastec.2004.08.015](https://doi.org/10.1016/j.optlastec.2004.08.015)
- [18] Ancona, A., Sibillano, T., Lugara, P. M., Gonnella, G., Pascasio, G., Maffione, D.: *J. Phys. D: Appl. Phys.*, 39, 2006, p. 563. [doi:10.1088/0022-3727/39/3/022](https://doi.org/10.1088/0022-3727/39/3/022)
- [19] Cao, X., Jahazi, M.: *Journal of Optics and Lasers in Engineering*, 47, 2009, p. 1231. [doi:10.1016/j.optlaseng.2009.05.010](https://doi.org/10.1016/j.optlaseng.2009.05.010)
- [20] Torkamany, M. J., Hamed, M. J., Malek, F., Sabbaghzadeh, J.: *Journal of Physics D: Applied Physics*, 39, 2006, p. 4563. [doi:10.1088/0022-3727/39/21/009](https://doi.org/10.1088/0022-3727/39/21/009)
- [21] Xiao-Long Gao, Jing Liu, Lin-Jie Zhang, Jian-Xun Zhang: *Materials Characterization*, 93, 2014, p. 136. [doi:10.1016/j.matchar.2014.04.005](https://doi.org/10.1016/j.matchar.2014.04.005)
- [22] Akman, E., Demir, A., Canel, T., Sımmazcelik, T.: *J. Mater. Process. Technol.*, 209, 2009, p. 3705. [doi:10.1016/j.jimatprotec.2008.08.026](https://doi.org/10.1016/j.jimatprotec.2008.08.026)